ISSN: 3029-0724

Research Article

Journal of Environmental Science and Agricultural Research

Drug Designing and Molecular Dynamics Identifies Cyanobacterial Nodularin-R as the Candidate Molecule Against SARS–CoV–2 Main Protease (Mpro)

Fahim Bashir[1*], Arif Bashir[2], Shabir Ahmad Ganai[3] and Sayyed RZ[4*]

[1]*Department of Environmental Science, University of Kashmir, Srinagar, 190006, India*
[2]*Department of Clinical Biochemistry, Government College for Women, Nawa-Kadal, Srinagar, India*
[3]*Division of Basic Sciences and Humanities, FoA, SKUAST-Kashmir, 193201, Jammu and Kashmir, India*
[4]*Faculty of Health and Life Sciences, INTI International University, Persiaran Perdana BBN, Putra Nilai, 71800 Nilai, Negeri Sembilan, Malaysia*

[*]**Corresponding author**
Fahim Bashir and Sayyed RZ, Department of Environmental Science, University of Kashmir, Srinagar, 190006, India.
Sayyed RZ, Faculty of Health and Life Sciences, INTI International University, Persiaran Perdana BBN, Putra Nilai, 71800 Nilai, Negeri Sembilan, Malaysia.

Received: June 02, 2025; **Accepted:** June 12, 2025; **Published:** June 18, 2025

ABSTRACT

The COVID-19 pandemic, caused by SARS-CoV-2, is a significant public health challenge. One approach to combat this virus is to develop antiviral drugs from natural products, such as those produced by cyanobacteria. Cyanobacteria produce a diverse range of secondary metabolites (SMs), including nodularin, aplysiatoxin, and obyanamide, which have unique chemical properties that make them potential scaffolds for drug development. We hypothesized that these SMs might be effective binders against the main protease of SARS-CoV-2, a key target for antiviral therapy. To test this, we used structure-guided drug design tactics to investigate the binding affinity of 13 cyanobacterial SMs against the main protease. Our results showed that three metabolites - nodularin-R, aplysiatoxin, and obyanamide had the highest binding affinity towards the main protease. We further analyzed the interaction profiles of these molecules in a bound state with the main protease. Notably, we calculated the binding free energies of nodularin-R using molecular mechanics/generalized born surface area (MM-GBSA) and free energy landscape (FEL) analysis, along with molecular dynamics (MD) simulations. These simulations demonstrated the stability of nodularin-R in the active site of the main protease. Our study suggests that nodularin-R may be a promising therapeutic against SARS-CoV-2, pending further clinical evaluation. This research highlights the potential of cyanobacterial SMs as a rich source of antiviral compounds and demonstrates the power of structure-guided drug design in identifying promising leads.

Keywords: Specialized Metabolites, Binding Affinity, MD Simulations, Molecular Docking, Molecular Dynamics

Introduction

The 2019-novel coronavirus (2019-nCov), responsible for the pandemic coronavirus disease 2019 (COVID-19) belongs to the subfamily of Orthocoronavirinae, family Coronavidae, order Nidovirales, and the genus Betacoronavirus that affects animals and mammals [1]. It caused a global pandemic since 2019 that is still ongoing, leading to millions of infections and deaths, and economic crises worldwide [2]. Till 7 October 2021, the number of confirmed cases of COVID-19 is 236,132,082 with 4,822,472 deaths (World health organization (WHO) global statistics). Furthermore, until this date, a total of 6,262,445,422 vaccine doses have been administered (WHO global statistics). In addition to vaccination, therapeutic options against this 2019 novel coronavirus remain a major challenge for the scientific and medical community. The genome of this coronavirus consists of 11 open reading frames ORFs (reference sequence: NC_045512.2, severe acute respiratory syndrome coronavirus

Citation: Fahim Bashir, Arif Bashir, Shabir Ahmad Ganai, Sayyed RZ. Paleoecologic Reconstructions for Crimean Cretaceous-Paleogene Boundary. J Envi Sci Agri Res. 2025. 3(3): 1-12. DOI: doi.org/10.61440/JESAR.2025.v3.58

2 isolate Wuhan-Hu-1, complete genome). The size of these genes are as follows: ORF1ab is 21,290 bp in length, S gene is 3,822 bp, ORF3a is 828 bp, E gene is 228 bp, M gene is 669 bp, ORF6 is 186 bp, ORF7a is 366 bp, ORF7b is 132 bp, ORF8 is 366 bp, N gene is 1,260 bp and lastly ORF10 is 117 bp in length [3]. The proteins encoded by these ORFs are as follows: Replicase polyprotein 1ab (P0DTD1), Replicase polyprotein 1a (P0DTC1), Spike glycoprotein (P0DTC2), ORF3a protein (P0DTC3), Envelope small membrane protein (P0DTC4), Membrane protein (P0DTC5), ORF6 protein (P0DTC6), ORF7a protein (P0DTC7), ORF7b protein (P0DTD8), ORF8 protein (P0DTC8), Nucleoprotein (P0DTC9) and ORF10 protein (A0A663DJA2) respectively, as per Uniprot database accession numbers [4]. Since the start of the pandemic, several research groups have aimed to develop antiviral drugs against 2019-nCov by targeting the extracellular proteases such as ACE-2, TMPRSS2, Furin, intracellular proteases including Cathepsin L, SARS-Co-V2 spike proteins, RNA dependent RNA Polymerase, Papain-like protease (PLpro), and Main Protease (Mpro) [5].

Currently, rapid vaccine development has halted the spread of the virus globally. However, the appearance of new mutants that could resist the different approved vaccines worries more and more the scientific community as long as no effective treatment has been approved. To prevent outbreaks by novel mutant strains of this severe acute respiratory syndrome 2019-novel coronavirus or SARS-CoV-2, the effort of the scientific community is currently focusing on developing specific antiviral agents that are effective against this 2019-nCov. One of the SARS-CoV-2 drug targets is the Mpro which is also named 3-Chymotrypsin like Protease or non-structural protein 5 [6]. This protease enzyme is generated from the translation of ORF1ab, and it cleaves the viral protein replicase polyprotein to generate the non-structural proteins 4, 6-16, which are essential for the viral particles to assemble and replicate inside the host cell [7]. The Mpro cleaves ORF1ab at certain specific amino acid sites and its functional protein is a dimer, each subunit is composed of three domains I, II, and III. Its substrate-binding site is located between the first two domains and comprises the unique catalytic dyad (Cys 145 - His 41), which is lacking in human proteases [8]. Therefore, Mpro is one of the promising drug targets for SARS-CoV-2, as it has unique sites for recognizing the amino acids for cleavage, which are not present in the proteases of humans.

Natural compounds-based drugs derived from living organisms are traditionally used in human therapy and are gaining importance in the modern world healthcare sector. Due to their extraordinary abundance in the marine environment and their production of a large diversity of SMs, cyanobacteria have attracted the attention of many research groups worldwide as a highly potential source of new pharmaceutically active compounds [9]. Several literature studies (Table 1) have reported antiviral, antifungal, antibacterial, anticancer, anti-inflammatory, and antioxidant activities of cyanobacterial metabolites [10,11]. Recently, studies exploring algae and cyanobacteria as promising natural sources of the antiviral drug against SARS-CoV-2 have been reported [12]. These studies revealed that cyanobacterial metabolites such as flavonols, flavanones, and alkaloids showed potential inhibitor activity against coronavirus proteins like transmembrane protease serine 2 (TMPRSS2), main protease (Mpro), and angiotensin-converting enzyme 2 (ACE2) involved in SARS-CoV-2 viral replication [13]. Similarly, microginins, a class of linear peptides produced by the cyanobacterial genus Microcystis, showed potential inhibitor activity against ACE [11]. Given the urgent need to block the SARS-CoV-2 pandemic worldwide and the years of research and development required for the discovery of new effective drugs by a conventional approach, there has been considerable interest in both the reuse of approved antiviral agents and in silico drug repurposing approach based on molecular docking of natural products from various microorganisms [14]. Due to the rapid genomic sequencing of SARS-CoV-2 and the identification of drug-binding pockets of key viral enzymes essential for virus replication, such as the major protease (Mpro) and papain-like protease (PLpro), the in silico molecular interaction-based approach could rapidly lead to the discovery of a potential drug against existing and future emerging 2019-nCov mutants. In this study, we investigated thirteen cyanobacterial metabolites by targeting the Mpro protease of 2019-nCov using this in silico approach based on molecular docking.

Materials and Methods

Selection of Cyanobacterial Metabolites for the Study

Structure coordinates of thirteen cyanobacterial metabolites were accessed from the fabled database PubChem [15]. The chemical structures have been provided in Figure 1. Two-dimensional coordinates of all the metabolites (ligands) were retrieved after confirming their various details. All the ligands were kept ready for subsequent molecular docking in a structure data file (SDF) format.

Selection of SARS-CoV-2 Main Protease Structure

Among the various crystal structures Available for SARS-CoV-2 main protease, we selected a structure bearing PDB ID: 6ZRU [16]. As a thumb rule before initiating molecular docking, we inspected the structure for any missing amino acid residues. Redundant molecules including native ligands associated with the protein chain of the main protease were removed. Maestro which is not only a user interface but performs other functions as well was used for checking the sequence continuity and for removing above mentioned irrelevant structures [17,18].

Docking Metabolites Against Processed Sars-Cov-2 Main Protease

CB-Dock server was used to perform molecular docking. Following the detection of putative binding regions, CB-Dock performs cavity sorting to detect the various top cavities based on their size [17,19]. Each ligand was docked against the main protease of SARS-CoV-2 individually. While the ligands were given as input in SDF format, the main protease was provided to the server as a PDB file. The docking centre was set, and the size of the docking box was adjusted. Finally, the molecular docking and reranking were performed with the help of Auto Dock Vina (version 1.1.2) [20]. CB-Dock server, as a default, performed docking in five putative cavities. The correct cavity in SARS-CoV-2 and the correct pose of ligands was assured and selected by taking advantage of native (cocrystallized)-ligand. As the binding region of the co-crystallized ligand has been determined experimentally, thus it serves as a good reference for confirming the correct binding site and poses of algorithm-docked ligands [17]. All thirteen docked complexes were minutely analyzed for picking the correct pose bound at the proper binding region. For this confirmation, the Chimera tool was employed [21].

Ligand-Main Protease Interaction Profile Study

From the docked complexes, the interaction profile was generated using the correct pose. The three-dimensional interaction profiles were generated through the protein-ligand interaction profiler. This tool explores interactions (non-covalent ones) between a ligand and its biological macromolecular target. Using the protein-ligand docked complex as input, this tool identifies seven interaction types between the duo at the atomistic scale. These interactions include not only hydrogen and hydrophobic contacts but also pi-cation, pi-stacking, water bridges, and salt bridges. Additionally, halogen bonds between the macromolecular target and ligand are also detected by this rule-based algorithm-reliant tool [17,22].

Molecular Dynamics Simulation

For checking the stability of Nodularin-R in the binding site of SARS-COV-2 main protease molecular dynamics (MD) simulation was performed. We used Desmond, a module of Schrödinger, for this purpose. The docked protein-ligand complex was preprocessed with the Protein Preparation Wizard of Maestro, where molecular optimization and energy minimization were done. After that, System Builder was used for system preparation, adding water for solvation, 0.15 M of sodium chloride (NaCl) and additional Na+/Cl- ions to neutralize the charges in the protein. Simple point-charge (SPC) was used as the water model. An orthorhombic box of 10 Å × 10 Å × 10 Å was adopted for simulation. An NPT ensemble with temperature of 300.0 K and pressure of 1.01325 bar was utilized.

Root means square deviation (RMSD), root mean square fluctuation (RMSF) and radius of gyration (Rg) were calculated using GROMACS. The Desmond trajectory is converted to the GROMACS, XTC format using MDTraj [23]. The commands gmx rms, gmx rmsf and gmx gyrate were used for RMSD, RMSF and Rg, respectively. For RMSD and RMSF, only the C-alpha atoms were considered, while for Rg, only the protein backbone was considered.

Principal Component Analysis and Free Energy Landscape

Principal component analysis (PCA) was used for the investigation of conformational change during the simulation. For PCA, the covariance matrix was calculated using only the C-alpha atomic coordinates of the protein. Diagonalizing the matrix, we obtained the eigenvectors (principal components) and the corresponding eigenvalues. In this process, GROMACS was employed. The XTC trajectory obtained before was input. The gmx covar and gmx anaeig commands were used for construction of the covariance matrix and diagonalization, respectively.

Free energy landscape (FEL) was to study the change of free energy and for the detection of metastable conformations. GROMACS was again utilized to calculate the Gibbs free energy as a function of the first two principal components (PCs), where the gmx sham command was used. Locally estimated scatterplot smoothing (LOESS) regression was used for smoothing the FEL plot.

Dynamic Cross-Correlation Matrix

Dynamic cross-correlation matrix (DCCM) was employed for studying the correlation in motions among different residues. Only the displacement of the C-alpha atom was considered in DCCM for each residue. The formula for calculating the correlation *C(i,j)* between the ith and jth residues is:

$$C(i,j) = \frac{< \Delta r_i \cdot \Delta r_j >}{<|\Delta r_i|^2>^{\frac{1}{2}} <|\Delta r_j|^2>^{\frac{1}{2}}}$$

In this formula, $\Delta \boldsymbol{r}_i$ is the displacement vector of the ith residue, and $|\Delta \boldsymbol{r}_i|$ denotes the length of the corresponding vector, and $\Delta \boldsymbol{r}_i \cdot \Delta \boldsymbol{r}_j$ represents the dot product of the two vectors, and the angle brackets represent the average value of the quantities. Positive correlation, negative correlation and no correlation are represented by $C(i,j)>0$, $C(i,j)<0$ and $C(i,j)=0$, respectively.

We used the dccm function in the Bio3D package [58,59] for calculation of DCCM. The DCD format of trajectory required for the dccm function was obtained using MDTraj, which can covert Desmond trajectory to different other formats.

Molecular Mechanics/Generalized Born Surface area (MM/GBSA) Energy

Molecular mechanics/generalized Born surface area (MM/GBSA) energy was calculated to evaluate the binding energy between the protein and the ligand. Uni-GBSA was employed for calculation of MM/GBSA energy [24]. This tool uses gmx_MMPBSA and MMPBSA.py of Amber for MM/GBSA calculation. The Desmond trajectory is separated into frames. For each frame, water and ions are removed, and the protein-ligand complex is split into two PDB files, one protein PDB and one ligand PDB. Open Babal was used to convert the ligand PDB file into MOL2 format. The protein PDB and ligand MOL2 were used as input of Uni-GBSA, where we used the default configuration file (default.ini, see https://github.com/dptech-corp/Uni-GBSA), after which the total free energy of binding is output.

Results

In silico Binding Interaction Studies of Selected Cyanobacterial Compounds with 2019-nCov Main Protease (Mpro).

The 13 cyanobacterial metabolites (Figure 1) were selected based on the previous reports of their potent biological effects, and some of them have antiviral activity (Table 1). All compounds were docked into the active site pocket of SARS CoV-2 Main protease (Mpro).

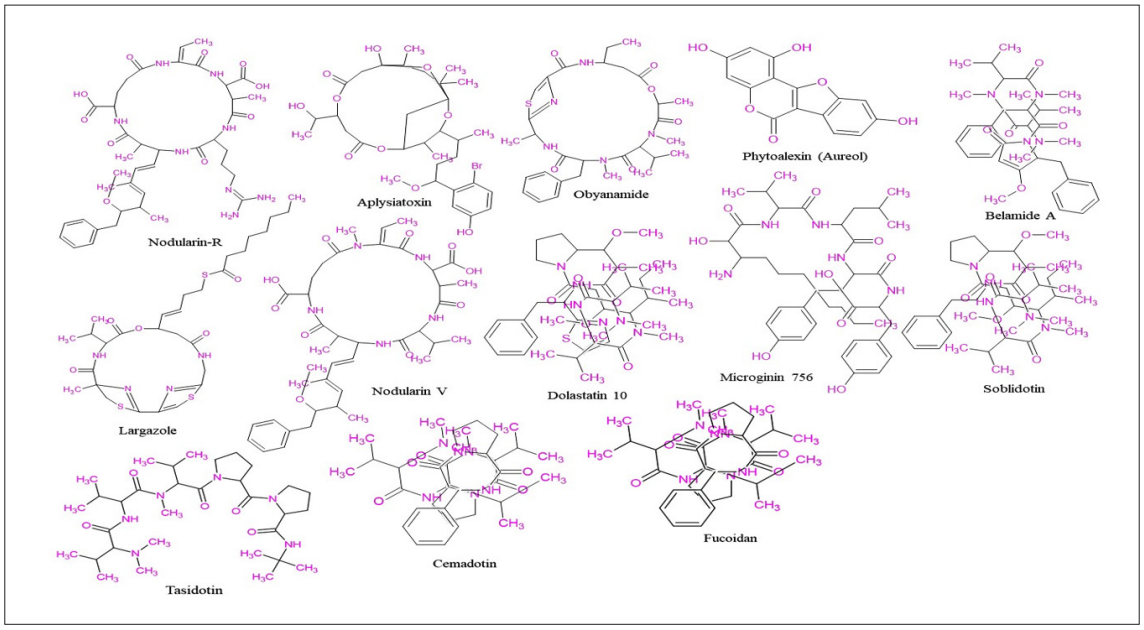

Figure 1: Structures of the 13 selected cyanobacterial metabolites, From the left to the right: Nodularin-R, Aplysiatoxin, Obynamide, Phytolexin, Belamide A, Largozole, Nodularin V, Dolastatin 10, Microginin 756, Soblidotin, Tasidotin, Cemadotin, and Fuciodan

Table 1: Biological activities of some cyanobacterial metabolites

Metabolites	Cyanobacteria	Biological Activity	References
Nodularin-R	Nodularia sp.	Protein phosphatase-1 inhibitor, cytotoxic	25
Nodularin-V (motuporin)	Theonella swinhoei	Protein phosphatase-1 inhibitor, cytotoxic	25,26
Aplysiatoxin	Lyngbya majuscula, Schizothrix calcicola, Oscillatoria nigro-viridis, Trichodesmium erythaeum	Antiviral activity	27
Obyanamide	Lyngbya confervoides	Anticancer activity	28
Phytoalexin	Scytonema ocellatum	Antifungal activity	29
Belamide A	Symploca sp.	Anticancer activity	30
Largazole	Symploca sp.	Anticancer and antiproliferative	31
Dolastatin 10	Dolabella auricularia	activities	32
Microginin 756	Microcystis sp.	Anticancer activity Inhibit angiotensin-converting	11, 33
Soblidotin	Dolabella auricularia	enzyme, potential	34
Tasidotin	Dolabella auricularia, and cyanobacteria	inhibitor of SARS-CoV-2	35
Cemadotin	D. auricularia/Symploca sp.	Anticancer activity	36
Fucoidan	Eclonia cava, and Costaria costata	Anticancer activity Antiviral, anticancer, and antimetastatic activities	37

Figure 2 shows the docking score (binding energy in kcal/mol) of the 13 selected cyanobacterial bioactive compounds with binding site amino acid residues of the SARS-CoV-2 Main protease (Mpro).

Molecular docking, basically a molecular modeling method has critical importance in finding atomic-level interactions between proteins and ligands [38]. Apart from this, how a ligand fits in the binding pocket of a biological macromolecule is also explored by this technique [39]. Cavity-detection guided Blind Docking (CB-Dock) server employs the empirical scoring function of Auto Dock Vina, which is majorly machine learning, for quantifying ligand-receptor affinity17, 20. A more negative value or lowest Vina Score indicates more binding affinity while the least negative or highest score designates the least ligand-receptor affinity. Our results

(Figure 2) show that nodularin-R docked with the best score or binding energy of −8.3 kcal/mol followed by aplysiatoxin (−8.0 kcal/mol), obyanamide (−7.9 Kcal/mol), phytoalexin (−7.3 Kcal/mol), belamide A (−7.1 Kcal/mol), largazole, nodularin-V, and dolastatin 10 (−7.0 Kcal/mol), microginin 756 (−6.6 Kcal/mol), soblidotin (−6.5 Kcal/mol), tasidotin (−6.3 Kcal/mol), cemadotin (−6.1 Kcal/mol), and fucoidan (−5.3 Kcal/mol) (Table S1). Recently, Pendyala et al. reported that among 16 phytochemicals screened by molecular docking against SARS-CoV-2 Main protease (Mpro), cyanobacterial phycocyanobilin showed also the highest docking score (−8.6 kcal/mol) [40].

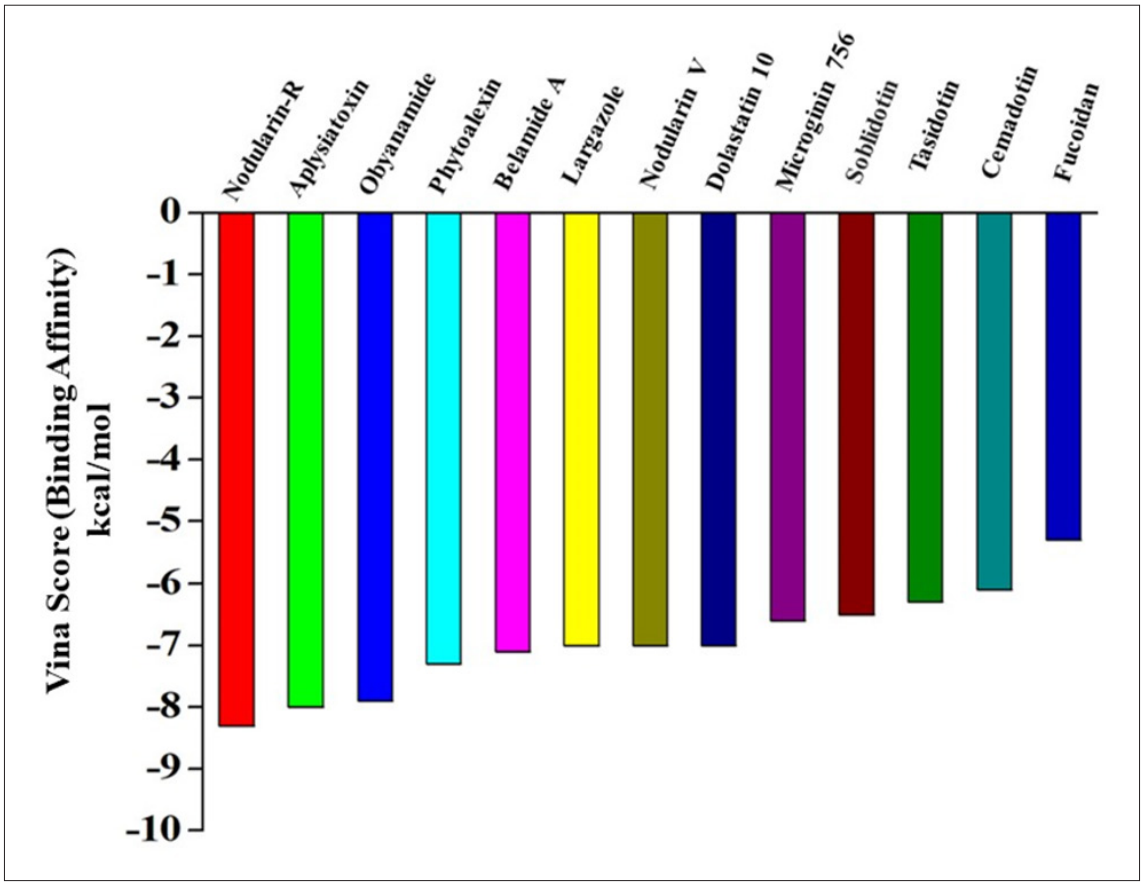

Figure 2: The binding affinity (vina score) of the 13 selected cyanobacterial metabolites towards the main protease (Mpro) of 2019-nCov. Interactions profiles of the highest affinity potential inhibitors (nodularin-R, aplysiatoxin, and obyanamide) with the binding pocket of the main protease (Mpro) of 2019-nCov

Ten key active-site amino acid residues (His 41, His 164, Asn 142, Gly 143, Arg 188, Gln 189, Gln 192, Pro 168, Thr 25, and Met 49) of 2019-nCov Mpro involved in polar interactions at a distance of < 5 Å with nodularin-R. However, only four (His 163, Glu 166, Gln 189, and Met 165) and three (Glu 166, Gln 189, and Met 49) key active-site amino acid residues involved in polar interactions at a distance of < 4 Å with aplysiatoxin and obyanamide, respectively. Specific polar contacts of each cyanobacterial compound are shown in Table 2. Recently, Amin et al.41 reported the list of key active-site amino acids (His 41, His 163, His 164, Cys-145, Met 49, Met 165, Gly 143, Ser 144, Glu 166, Leu 167, Asp 187, Arg 188, Gln 189, Gln 192, Thr 190, and Ala 191) involved in catalysis and substrate binding for Mpro of 2019-nCov. Our results also showed polar interactions in this specific substrate-binding region for the three potential inhibitors: nodularin-R, aplysiatoxin, and obyanamide [41].

Figures 3−5 show a 3-D representation of the binding pocket of the main protease (Mpro) of 2019-nCoV-2 with nodularin-R, aplysiatoxin, and obyanamide, respectively. Interaction profiles extracted from these three top-affinity showing docked complexes revealed especially hydrophobic and hydrogen bonding interactions between this protease and the ligands (Table 2). Among these three potential inhibitors, nodularin-R showed a better interaction profile compared to aplysiatoxin and obyanamide. In addition to a pi-cation interaction, it makes 5 hydrophobic and 9 hydrogen bonding interactions with specific amino acid residues located at the active site of the pocket of the Mpro. Certain residues like Asn 142 and Arg 188 were found to interact with nodularin-R through double hydrogen bonds. Several studies reported that both hydrophobic interactions and hydrogen bonding have cross-talk with stabilizing ligands in the binding pocket of proteins [42].

Table 2. Molecular Docking Results of Nodularin-R, Aplysiatoxin, and Obyanamide and their Interactions With Key-Active Site Amino Acid Residues Of 2019-Ncov Main Protease (Mpro)

Compounds		2019-nCov M^{pro}		
	Vina Score (kcal/mol)	H-bonding Contacts	Hydrophobic contacts	pi-cation contact
Nodularin-R	−8.3	His 41, Asn 142*, Gly 143, His 164, Arg 188*, Gln 189, Gln 192	Gln 192, Pro 168, Thr 25, Met 49, Gln 189	His 41
Aplysiatoxin	−8	His 163	Glu 166, Gln 189, Met 165	-
Obyanamide	−7.9	Glu 166*	Gln 189, Met 49	-

* Represents two hydrogen bonds

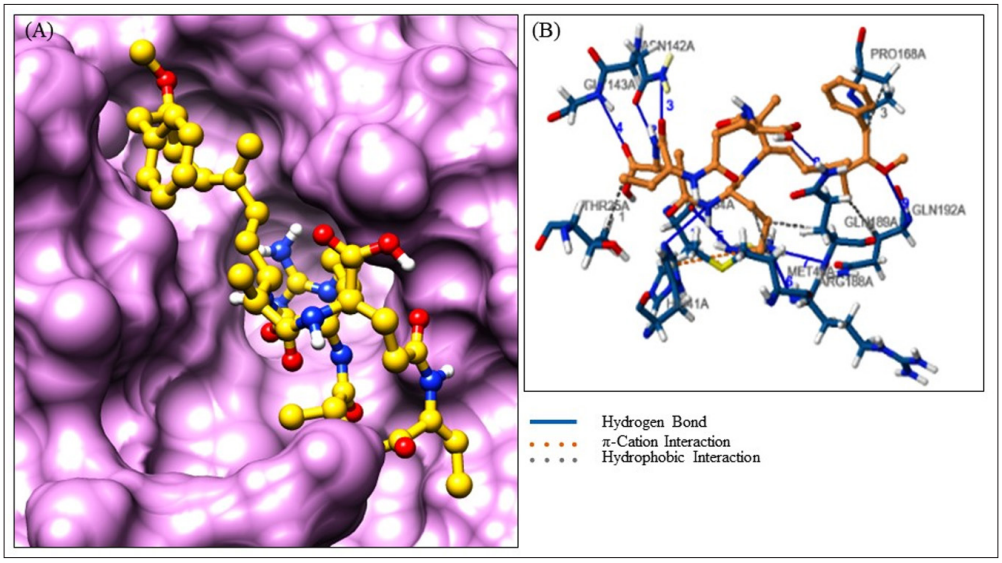

Figure 3: Mode of interaction of nodularin-R with the main protease (Mpro) of 2019-nCoV-2

(A) nodularin-R (yellow color) in the binding pocket of the Mpro (plum surface). (B) A 3-D docking pocket of 2019-nCov Mpro with nodularin-R (brown color), showing detailed ligand atom interactions with key-active site amino acid residues of Mpro. Nine hydrogen bonds (blue line), five hydrophobic bonds (dashed grey line), and one pi-cation interaction (dashed brown line) were observed between the ligand-receptor.

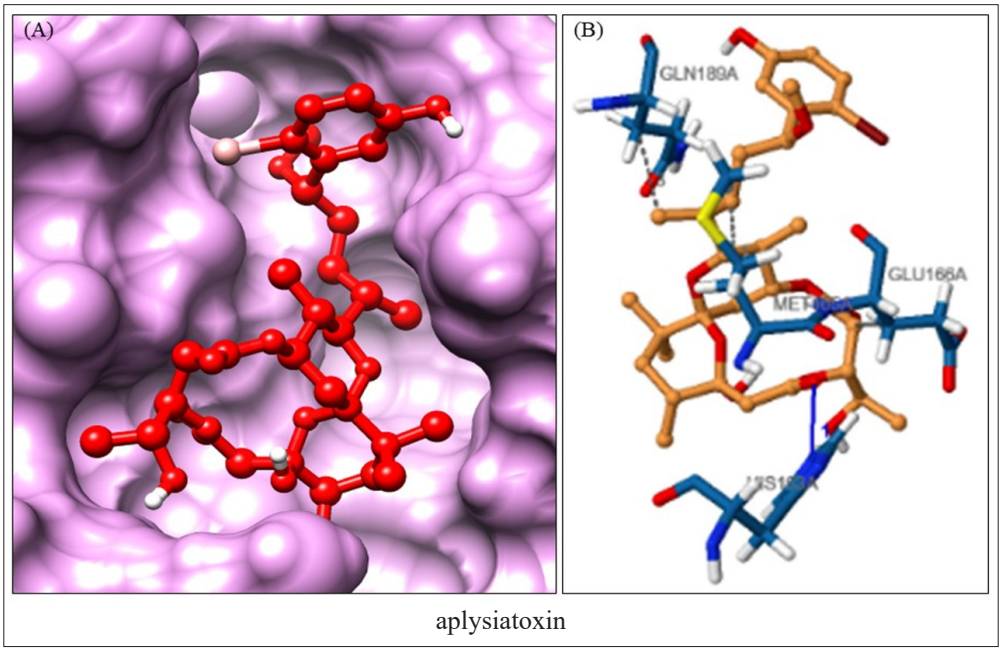

Figure 4: Mode of interaction of aplysiatoxin with the main protease (Mpro) of 2019-nCoV-2

(A) aplysiatoxin (red color) in the binding pocket of the Mpro (plum surface). (B) A 3-D docking pocket of 2019-nCov Mpro with aplysiatoxin (brown color), showing detailed ligand atom interactions with key-active site amino acid residues of Mpro. One hydrogen bond (blue line) and three hydrophobic bonds (dashed grey line) interactions were observed between the ligand-receptor.

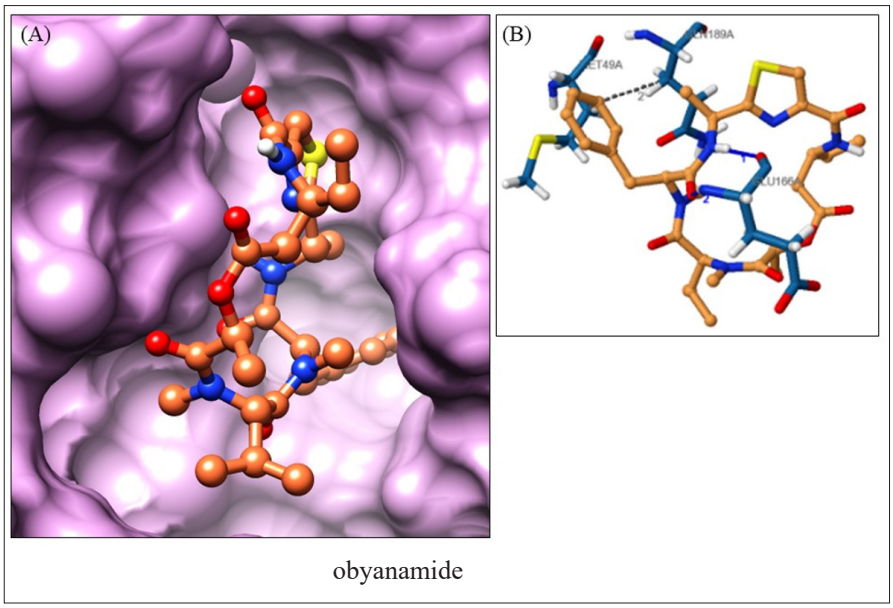

Figure 5: Mode of interaction of obyamide with the main protease (Mpro) of 2019-nCoV-2.

(A) obyanamide (brown color) in the binding pocket of the Mpro (plum surface). (B) A 3-D docking pocket of 2019-nCov Mpro with obyanamide (brown color), showing detailed ligand atom interactions with key-active site amino acid residues of Mpro. Two hydrogen bonds (blue line) and two hydrophobic bonds (dashed grey line) interactions were observed between the ligand-receptor.

Molecular Dynamics Manifested Stability Of Nodularin-R In the Groove of the Main Protease

To evaluate the reliability of the molecular docking and stability of the nodularin-R-Mpro docked complex, we conducted molecular dynamics (MD) simulations. The trajectories obtained from the complex were analyzed and plotted in terms of root mean square deviation (RMSD), root mean square fluctuation (RMSF), radius of gyration (Rg), principal component analysis (PCA), free energy landscape (FEL), dynamic cross-correlation matrix (DCCM) and molecular mechanics/generalized born surface area (MM/GBSA).

The RMSD the protein in nodularin-R-Mpro complex shows the degree of fluctuation of the protein during the MD simulation. During the 100 ns MD simulation, the RMSD values change abruptly initially, but it quickly equilibrated after 10 ns, with a mean of 1.898 Å and an SD of 0.274 Å. (Figure 6). The low RMSD value shows that the complex does not fluctuate much overall and it is an indication of its stability.

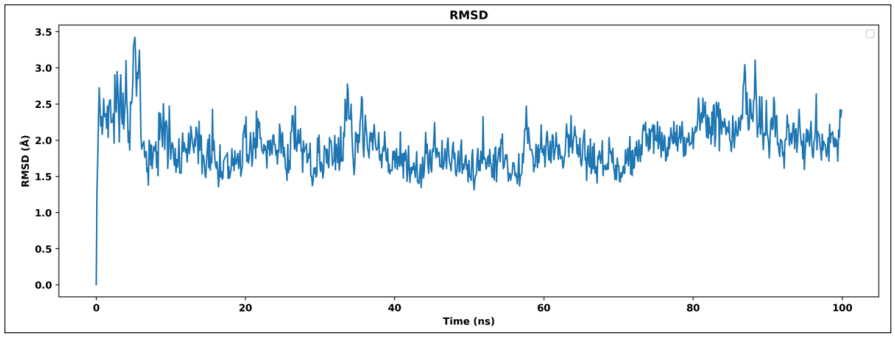

Figure 6: Root means square deviation (RMSD) of the protein in the nodularin-R-Mpro complex

The RMSF shows the local fluctuation of each residue of the protein in the nodularin-R-Mpro complex. In general, the fluctuation of the complex is low for most domains of the protein with RMSF values of lower than 3 (Figure 7). However, it is observed that the regions near the N- and C-terminal have relatively high RMSFs, probably because they are the free ends of the protein.

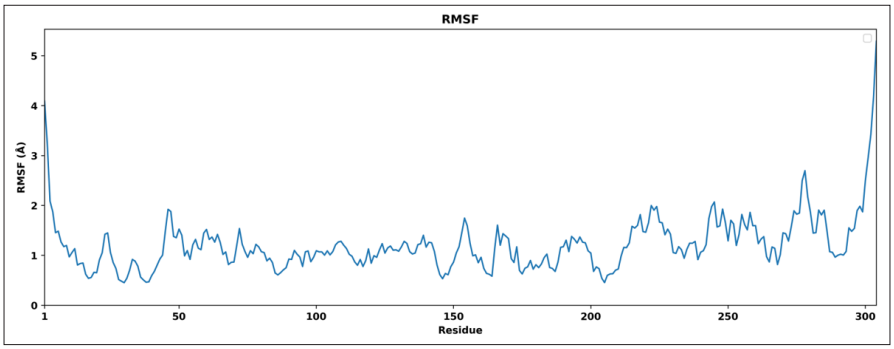

Figure 7: Root mean square fluctuation (RMSF) of the protein in the nodularin-R-Mpro complex

The Rg shows the level of compactness of protein. In the nodularin-R-Mpro complex, it shows that initially the Rg fluctuates, but after 40 ns, the values stabilize (mean: 21.93 Å, SD: 0.099 Å) (Figure 8). This shows that the degree of compactness does not change much and the complex attains equilibrium after some time in the simulation.

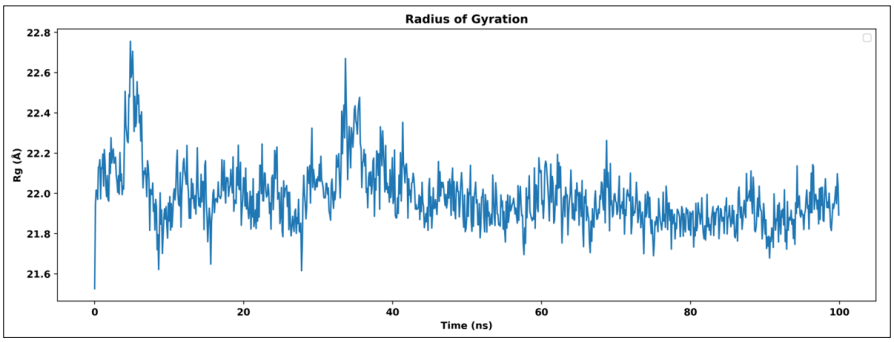

Figure 8: Radius of gyration (Rg) of the protein in the nodularin-R-Mpro complex

The conformational changes of the protein in the nodularin-R-Mpro complex are investigated via PCA and FEL. The PCA plot shows two dense regions where many dots accumulate, which suggests that there might be two metastable conformations (Figure 9). This is confirmed by the FEL plots, which shows the free energy of different conformations (Figure 10). It is shown that there exist two local minima of low energy, an indication of two stable conformations in the protein of the nodularin-R-Mpro complex.

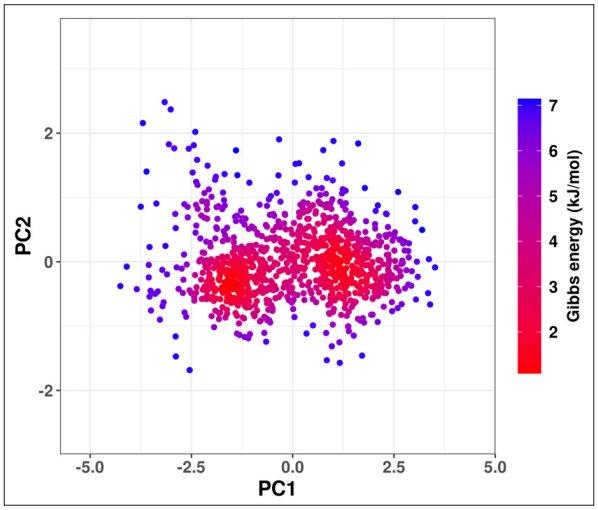

Figure 9: Principal component analysis (PCA) of the protein in the nodularin-R-Mpro complex

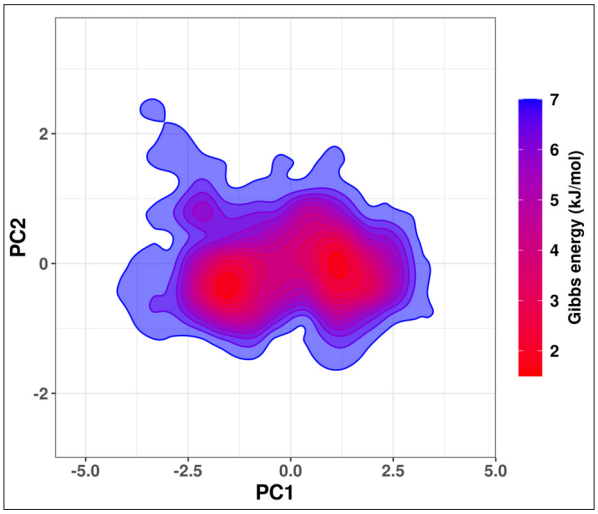

Figure 10: Free energy landscape (FEL) of the protein in the nodularin-R-Mpro complex

The DCCM analysis is used to investigate the correlation between the motions of different residues. Only the frames after 10 ns were considered since the RMSD results shows that the system attains equilibrium after that. The result shows that there are extensive correlations in motions in the protein of the nodularin-R-Mpro complex. The negative correlations are mainly found within residues 100-200 and between residue 20-100 and 200-250. The positive correlations are mainly between residues 100-200 and 20-100 and between residues 200-300 and 100-304 (Figure 11).

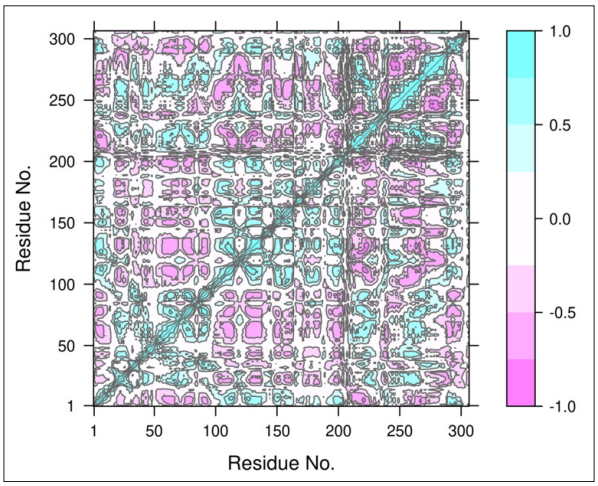

Figure 11: Dynamic cross-correlation matrix (DCCM) of the protein in the nodularin-R-Mpro complex

Molecular mechanics/generalized born surface area (MM/GBSA) was used to estimate the binding free energy between Mpro and nodularin-R in the protein-ligand complex. In the first 20 ns of the simulation, the MM/GBSA energy fluctuates, but after 20 ns, it stabilizes to a mean value of -28.63 kcal/mol (SD: 3.846 kcal/mol) (Figure 12). The large binding free energy indicates a stable protein-ligand interaction.

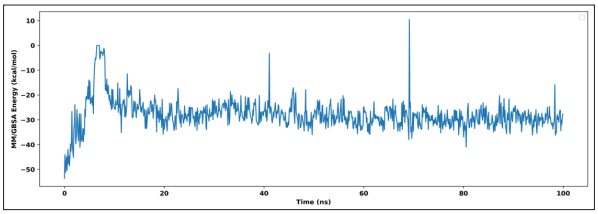

Figure 12: Molecular mechanics/generalized Born surface area (MM/GBSA) of the protein in the nodularin-R-Mpro complex

Molecular docking studies indicated that all nodularin-R residues (Adda, Glu, Mdhb, Asp, and Arg) are involved in polar interactions with key amino acid residues located at the active site of the pocket of the main protease of 2019-nCov. The Glu residue of nodularin-R is involved in a pi-cation interaction with the His 41 in the pocket of Mpro. The Arg, Mdhb, Glu, and Asp residues of nodularin-R interact by hydrophobic bonds with Arg 188, Asn 142, Gln 189, and Gly 143 in the pocket of Mpro, respectively. The residue Mdhb of nodularin-R interacts with the residue Asn 142 of Mpro through double hydrophobic bonds. In addition, all residues of nodularin-R are involved in hydrogen bond interactions with the Mpro' amino acid residues. Recently, Wu et al. reported that sequence alignment of Mpro of SARS-CoV-2 and other CoVs such as SARS-CoV and MERS are highly conserved, especially in the active site, which makes it a potential target for discovering new drugs against 2019-nCoV [43]. Our screening results by molecular docking performed on 13 metabolites of cyanobacteria suggest that nodularin-R is a promising inhibitory compound against the main protease 2019-nCoV. However, nodularin-R is also known as a powerful liver tumor promoter and potent inhibitor of the protein phosphatase-1 and -2A catalytic subunits [44]. The crystal structure study of the nodularin-R: PP1 complex showed that all amino acid residues of the toxin, except the Arg residue, involved also in polar interactions with key-active amino acid residues located at the active site of the pocket of the PP1 [45]. Therefore, the structure of nodularin-R could serve as a model for designing new anti-2019-nCoV active principles by modifying certain functional groups in its chemical structure to reduce its toxicity and increase its inhibitory potential against the main protease [46-56].

Discussion

Computational techniques play a crucial role in speeding up the discovery of new drugs, especially in times of global health crises like the COVID-19 pandemic. This study used molecular dynamics simulations to thoroughly analyze the stability, dynamics, and binding interactions of the nodularin-R-Mpro complex, revealing its potential as a strong inhibitor of SARS-CoV-2 major protease (Mpro). The nodularin-R-Mpro complex reached stability following an initial equilibration period, as demonstrated by the root mean square deviation (RMSD) analysis of the MD simulation data. With a mean RMSD of roughly 1.898 Å and a standard deviation of 0.274 Å, the complex showed notable overall little variation, indicating a strong and stable interaction between nodularin-R and Mpro during the MD simulation. Furthermore, localised variations within the protein-ligand complex, notably close to the N- and C-terminals, were identified by root mean square fluctuation (RMSF) analysis as suggestive of dynamic behaviour at these locations.

The nodularin-R-Mpro complex's conformational landscape was further clarified by principal component analysis (PCA) and free energy landscape (FEL) analysis, which showed the existence of two metastable conformations. These results highlight the possibility of several conformational states or binding modes, offering important new understandings of the dynamics and binding processes of the protein-ligand interaction. Furthermore, the examination of the dynamic cross-correlation matrix (DCCM) revealed significant correlations in the movements within the complex's protein, emphasising the coordinated movements of various residues during the simulation.

Molecular mechanics/generalized Born surface area (MM/GBSA) analysis, which revealed a stable protein-ligand interaction with a large negative binding free energy of roughly -28.63 kcal/mol, supporting a favourable binding affinity between nodularin-R and Mpro, provided evidence for the robust binding affinity between the two molecules. Molecular docking experiments confirmed nodularin-R's potential as a promising inhibitor of SARS-CoV-2 major protease by elucidating precise interactions between it and important amino acid residues in the active site pocket of Mpro.

These results highlight nodularin-R's therapeutic potential as a strong and stable inhibitor of SARS-CoV-2 main protease. Rigid preclinical and clinical studies are therefore required in order to establish its safety and efficacy for clinical use. By integrating computational methodologies with experimental validation, this study contributes to the accelerated development of effective antivirals against emerging infectious diseases like COVID-19, highlighting the pivotal role of computational drug design in addressing global health challenges.

Conclusions

In this report, thirteen SMs were investigated for their binding affinity towards the main protease of SARS-CoV-2. It was found that three metabolites (nodularin-R, aplysiatoxin, and obyanamide) proved best in terms of affinity against the defined protease. These molecules interacted with this protease through multiple interactions. Importantly, nodularin-R, the best-scoring molecule proved quite stable in the binding pocket of the main protease as it showed no drifting from an initial binding position. The bottom line of the study is that nodularin-R may prove as a potent and stable molecule for obstructing SARS-CoV-2 main protease. However, stringent clinical studies are required for promoting this marvelous molecule from ocean to bedside.

Supplementary Materials: Table S1: Vina score of different cyanobacterial metabolites against the main protease.

Author Contributions: FB, AB: Designing, interaction profile, rendering, writing, and outcome of experiments, SAG: Designing, molecular docking, and molecular dynamics, RZS: Manuscript editing and reviewing.

Informed Consent Statement: No human volunteers were involved in this research.

Availability of data and material: All the data are embedded in the manuscript and its supplementary file.

Conflicts of Interest: None

References

1. Wiam B. The Phylogeny of SARS Cov-2 (An Update of The Year 2022). university center of abdalhafid boussouf-MILA, 2022.
2. Acter T, Uddin N, Das J, Akhter A, Choudhury TR, Kim S. Evolution of severe acute respiratory syndrome coronavirus 2 (SARS-CoV-2) as coronavirus disease 2019 (COVID-19) pandemic: A global health emergency. Science of the Total Environment. 2020. 730: 138996.
3. Zekri AR, Amer KE, Hafez MM, Hassan ZK, Ahmed OS, et al. Genomic characterization of SARS-CoV-2 in Egypt. Journal of advanced research. 2021. 30: 123-32.
4. O'Donoghue SI, Schafferhans A, Sikta N, Stolte C, Kaur S, et al. SARS-CoV-2 structural coverage map reveals viral protein assembly, mimicry, and hijacking mechanisms. Molecular systems biology. 2021. 17: e10079.
5. Bandyopadhyay SS, Halder AK, Saha S, Chatterjee P, Nasipuri M, et al. Assessment of GO-based protein interaction affinities in the large-scale human–coronavirus family interactome. Vaccines. 2023. 11: 549.
6. Joshi S, Joshi M, Degani MS. Tackling SARS-CoV-2: proposed targets and repurposed drugs. Future medicinal chemistry. 2020. 12: 1579-601.
7. Martinez MA. Compounds with therapeutic potential against novel respiratory 2019 coronavirus. Antimicrobial agents and chemotherapy. 2020. 64.
8. Yadav R, Chaudhary JK, Jain N, Chaudhary PK, Khanra S, et al. Role of structural and non-structural proteins and therapeutic targets of SARS-CoV-2 for COVID-19. Cells. 2021. 10: 821.
9. Razali R, Asis H, Budiman C. Structure-function characteristics of SARS-CoV-2 proteases and their potential inhibitors from microbial sources. Microorganisms. 2021. 9: 2481.
10. Tiwari AK, Tiwari BS. Cyanotherapeutics: An emerging field for future drug discovery. Applied phycology. 2020. 1: 44-57.
11. Mondal A, Bose S, Banerjee S, Patra JK, Malik J, et al. Marine cyanobacteria and microalgae metabolites—A rich source of potential anticancer drugs. Marine Drugs. 2020. 18: 476.
12. Mazur-Marzec H, Cegłowska M, Konkel R, Pyrć K. Antiviral cyanometabolites—a review. Biomolecules. 2021. 11: 474.
13. Sami N, Ahmad R, Fatma T. Exploring algae and cyanobacteria as a promising natural source of antiviral drug against SARS-CoV-2. Biomedical Journal. 2021. 44:54-62.
14. Artese A, Svicher V, Costa G, Salpini R, Di Maio VC, et al. Current status of antivirals and druggable targets of SARS CoV-2 and other human pathogenic coronaviruses. Drug Resistance Updates. 2020. 53: 100721.
15. Kim S, Chen J, Cheng T, Gindulyte A, He J, He S, Li Q, Shoemaker BA, Thiessen PA, Yu B, Zaslavsky L. PubChem in 2021: new data content and improved web interfaces. Nucleic acids research. 2021. 49: D1388-95.
16. Oerlemans R, Ruiz-Moreno AJ, Cong Y, Kumar ND, Velasco-Velazquez MA, et al. Repurposing the HCV NS3–4A protease drug boceprevir as COVID-19 therapeutics. RSC medicinal chemistry. 2021. 12: 370-379.
17. Ganai SA. Characterizing binding intensity and energetic features of histone deacetylase inhibitor pracinostat towards class I HDAC isozymes through futuristic drug designing strategy. In Silico Pharmacology. 2021. 9: 1-8.
18. Mir MA, Ganai SA, Mansoor S, Jan S, Mani P, et al. Isolation, purification and characterization of naturally derived Crocetin beta-d-glucosyl ester from Crocus sativus L. against breast cancer and its binding chemistry with ER-alpha/HDAC2. Saudi Journal of Biological Sciences. 2020. 27: 975-84.
19. Liu Y, Grimm M, Dai WT, Hou MC, Xiao ZX, et al. CB-Dock: a web server for cavity detection-guided protein–ligand blind docking. Acta Pharmacologica Sinica. 2020. 41: 138-44.
20. Trott O, Olson A. Software news and update AutoDock Vina: Improving the speed and accuracy of docking with a new scoring function. Effic. Optim. Multithreading. 2009. 31: 455-61.
21. Pettersen EF, Goddard TD, Huang CC, Couch GS, Greenblatt DM, et al. UCSF Chimera—a visualization system for exploratory research and analysis. Journal of computational chemistry. 2004. 25: 1605-12.
22. Salentin S, Schreiber S, Haupt VJ, Adasme MF, Schroeder M. PLIP: fully automated protein–ligand interaction profiler. Nucleic acids research. 2015. 43: W443-W447. (23)
23. McGibbon RT, Beauchamp KA, Harrigan MP, Klein C, Swails JM, et al. MDTraj: a modern open library for the analysis of molecular dynamics trajectories. Biophysical journal. 2015 Oct 20;109(8):1528-32.
24. Yang M, Bo Z, Xu T, Xu B, Wang D, Zheng H. Uni-GBSA: an open-source and web-based automatic workflow to perform MM/GB (PB) SA calculations for virtual screening. Briefings in Bioinformatics. 2023. 24: bbad218.

25. Gulledge BM, Aggen JB, Huang H, Nairn AC, Chamberlin AR. The microcystins and nodularins: cyclic polypeptide inhibitors of PP1 and PP2A. Current medicinal chemistry. 2002. 9: 1991-2003.
26. De Silva ED, Williams DE, Andersen RJ, Klix H, Holmes CF, Allen TM. Motuporin, a potent protein phosphatase inhibitor isolated from the Papua New Guinea sponge Theonella swinhoei Gray. Tetrahedron letters. 1992. 33: 1561-1564.
27. Moore RE, Blackman AJ, Cheuk CE, Mynderse JS, Matsumoto GK, C, et al. Absolute stereochemistries of the aplysiatoxins and oscillatoxin A. The Journal of Organic Chemistry. 1984. 49: 2484-2489.
28. Gupta DK, Kaur P, Leong ST, Tan LT, Prinsep MR, et al. Anti-Chikungunya viral activities of aplysiatoxin-related compounds from the marine cyanobacterium Trichodesmium erythraeum. Marine drugs. 2014. 12: 115-27.
29. Han B-N, Liang T-T, Keen LJ, Fan T-T, Zhang X-D, et al. Two marine cyanobacterial aplysiatoxin polyketides, neo-debromoaplysiatoxin A and B, with K+ channel inhibition activity. Organic letters. 2018. 20: 578-581.
30. Chlipala GE, Tri PH, Hung NV, Krunic A, Shim SH, et al. Nhatrangins A and B, aplysiatoxin-related metabolites from the marine cyanobacterium Lyngbya majuscula from Vietnam. Journal of natural products. 2010. 73: 784-787.
31. Mynderse JS, Moore RE, Kashiwagi M, Norton TR. Antileukemia activity in the Osillatoriaceae: isolation of Debromoaplysiatoxin from Lyngbya. Science 1977. 196: 538-540.
32. Williams PG, Yoshida WY, Moore RE, Paul VJ. Isolation and structure determination of obyanamide, a novel cytotoxic cyclic depsipeptide from the marine cyanobacterium Lyngbya confervoides. Journal of natural products 2002. 65: 29-31.
33. Patterson GM, Bolis CM. Fungal cellwall polysaccharides elicit an antifungal secondary metabolite (phytoalexin) in the cyanobacterium scytonema ocelutum 2. Journal of Phycology. 1997. 33: 54-60.
34. Simmons TL, McPhai KL, Ortega-Barría E, Mooberry SL, Gerwick WH. Belamide A, a new antimitotic tetrapeptide from a Panamanian marine cyanobacterium. Tetrahedron Letters. 2006. 47: 3387-3390.
35. Taori K, Paul VJ, Luesch H. Structure and activity of largazole, a potent antiproliferative agent from the Floridian marine cyanobacterium Symploca sp. Journal of the American Chemical Society. 2008. 130: 1806-1807.
36. Liu Y, Salvador LA, Byeon S, Ying Y, Kwan JC, Law BK, et al. Anticolon cancer activity of largazole, a marine-derived tunable histone deacetylase inhibitor. Journal of Pharmacology and Experimental Therapeutics. 2010. 335: 351-361.
37. Madden T, Tran HT, Beck, D., Huie, R., Newman, R. A., Pusztai, L., Wright, J. J., Abbruzzese, J. L. Novel marine-derived anticancer agents: a phase I clinical, pharmacological, and pharmacodynamic study of dolastatin 10 (NSC 376128) in patients with advanced solid tumors. Clinical Cancer Research. 2000. 6: 1293-1301.
38. Paiva FC, Ferreira GM, Trossini GH, Pinto E. Identification, in vitro testing and molecular docking studies of microginins' mechanism of angiotensin-converting enzyme inhibition. Molecules. 2017. 22: 1884.
39. Watanabe J, Minami, M., Kobayashi, M. Antitumor activity of TZT-1027 (Soblidotin). Anticancer research. 2006. 26: 1973-1981.
40. Mita AC, Hammond LA, Bonate PL, Weiss G, McCreery H, S et al. B. Phase I and pharmacokinetic study of tasidotin hydrochloride (ILX651), a third-generation dolastatin-15 analogue, administered weekly for 3 weeks every 28 days in patients with advanced solid tumors. Clinical Cancer Research. 2006. 12: 5207-5215.
41. Supko JG, Lynch TJ, Clark JW, Fram R, Allen LF, et al. A phase I clinical and pharmacokinetic study of the dolastatin analogue cemadotin administered as a 5-day continuous intravenous infusion. Cancer Chemother Pharmacol. 2000. 46: 319-328,
42. Ermakova S, Sokolova R, Kim S-M, Um B-H, Isakov V, et al. Fucoidans from brown seaweeds Sargassum hornery, Eclonia cava, Costaria costata: structural characteristics and anticancer activity. Applied biochemistry and biotechnology. 2011. 164. 841-850.
43. Alekseyenko T, Zhanayeva SY, Venediktova A, Zvyagintseva T, Kuznetsova T, et al. Antitumor and antimetastatic activity of fucoidan, a sulfated polysaccharide isolated from the Okhotsk Sea Fucus evanescens brown alga. Bulletin of experimental biology and medicine. 2007. 143: 730-732.
44. Krylova NV, Ermakova SP, Lavrov VF, Leneva IA, Kompanets GG, et al. The comparative analysis of antiviral activity of native and modified fucoidans from brown algae Fucus evanescens in vitro and in vivo. Marine drugs. 2020. 18: 224.
45. Luthuli S, Wu S, Cheng Y, Zheng X, Wu M, Tong H. Therapeutic effects of fucoidan: a review on recent studies. Marine drugs. 2019. 17: 487.
46. Meng X-Y, Zhang H-X, Mezei M, Cui M. Molecular docking: a powerful approach for structure-based drug discovery. Curr Comput Aided Drug Des. 2011. 7: 146-157.
47. Ganai SA, Srinivasan P, Rajamanikandan S, Shah BA, Mohan S, et al. Delineating binding potential, stability of Sulforaphane-N-acetyl-cysteine in the active site of histone deacetylase 2 and testing its cytotoxicity against distinct cancer lines through stringent molecular dynamics, DFT and cell-based assays. Chemical biology & drug design. 2021. 98: 363-376.
48. Shah BA, Ganai SA, Koul AM, Mohan S, Amin A, et al. Exploring novel and potent molecules for disrupting DEPTOR-mTOR interaction through structure-steered screening, extra-exactitude molecular docking, prime binding free energy estimation and voguish molecular dynamics. Journal of biomolecular structure & dynamics. 2021. 1-11.
49. Pendyala B, Patras A, Dash C. Phycobilins as potent food bioactive broad-spectrum inhibitor compounds against Mpro and PLpro of SARS-CoV-2 and other coronaviruses: A preliminary Study. bioRxiv. 2020.
50. Amin SA, Banerjee S, Ghosh K, Gayen S, Jha T. Protease targeted COVID-19 drug discovery and its challenges: Insight into viral main protease (Mpro) and papain-like protease (PLpro) inhibitors. Bioorganic & medicinal chemistry. 2021. 29: 115860.

51. Patil R, Das S, Stanley A, Yadav L, Sudhakar A, et al. Optimized hydrophobic interactions and hydrogen bonding at the target-ligand interface leads the pathways of drug-designing. PLoS One. 2010. 5: e12029-e12029.
52. Wu C, Liu Y, Yang Y, Zhang P, Zhong W, et al. Analysis of therapeutic targets for SARS-CoV-2 and discovery of potential drugs by computational methods. Acta Pharmaceutica Sinica B. 2020. 10: 766-788.
53. Yoshizawa S, Matsushima R, Watanabe MF, Harada K.-i, Ichihara A, et al. Inhibition of protein phosphatases by microcystis and nodularin associated with hepatotoxicity. Journal of cancer research and clinical oncology. 1990. 116: 609-614.
54. Nishiwaki-Matsushima R, Ohta T, Nishiwaki S, Suganuma M, Kohyama K, et al. Liver tumor promotion by the cyanobacterial cyclic peptide toxin microcystin-LR. Journal of cancer research and clinical oncology. 1992: 118: 420-424.
55. Holmes CF, Boland MP. Inhibitors of protein phosphatase-1 and-2A, two of the major serine/threonine protein phosphatases involved in cellular regulation: Current Opinion in Structural Biology 1993, 3: 934–943. Current Opinion in Structural Biology. 1993. 3: 934-943.
56. Kelker MS, Page R, Peti W. Crystal structures of protein phosphatase-1 bound to nodularin-R and tautomycin: a novel scaffold for structure-based drug design of serine/threonine phosphatase inhibitors. Journal of molecular biology. 2009. 385: 11-21.